Giant, 5, 2021, 100040

Doxorubicin@ PEPylated interferon-polydisulfide: A multi-responsive nanoparticle for enhanced chemo–protein combination therapy

Hao Wang[a], **Yali Hu**[a,b], **Yaoyi Wang**[a], **Jianhua Lu**[a], **Hua Lu**[a,*]

[a] Beijing National Laboratory for Molecular Sciences, Center for Soft Matter Science and Engineering, Key Laboratory of Polymer Chemistry and Physics of Ministry of Education, College of Chemistry and Molecular Engineering, Peking University, Beijing 100871, China
[b] Peking-Tsinghua Center for Life Sciences, Academy for Advanced Interdisciplinary Studies, Peking University, Beijing 100871, China

Keywords: PEPylation, Polydisulfide, Chemo-protein combination therapy, Interferon, Doxorubicin

The combination of chemotherapy and protein therapy holds immense promise for tumor treatment. However, conventional bolus formulation or simple co-administration fails to achieve maximized efficacy due to the distinct physiological and pharmacological properties of small molecular drugs and protein therapeutics. As such, developing a co-delivery system for optimal antitumor efficacy remains a great challenge. Herein, we achieve the synergistic co-delivery of human interferon-α2b (IFN) and doxorubicin (Dox) by the facile synthesis of a multifunctional and stimuli-responsive protein-drug-polymer (PDP) conjugate IFN-PolyDox-PEP. IFN-PolyDox-PEP is constituted of IFN, a polydisulfide tethering multiple copies of Dox (PolyDox), and a stealthy polypeptide (PEP) for long circulation. IFN-PolyDox-PEP self-assembles into nanoparticles of 122 nm in diameter and is able to release its therapeutic cargos in response to tumor microenvironment cues such as matrix metalloproteinase, acidic pH, and reducing glutathione. The *in vivo* synergistic effect of IFN-PolyDox-PEP is demonstrated by the superior antitumor efficacy as compared with the co-administration of IFN-polypeptide conjugate and free Dox. This work demonstrates the power of highly efficient chemistry in constructing well-defined PDP conjugates, which are promising hybrid macromolecules for various chemo-protein combination therapies.

Introduction

Both small molecular chemotherapy drugs and macromolecular biologics are widely used for the treatment of cancers. However, both classes suffer from their own intrinsic limitations. For example, the pharmacological activities of protein drugs are often hampered by their poor proteolytic and thermal stability, lack of

* Corresponding author.
E-mail address: chemhualu@pku.edu.cn (H. Lu).
Received 10 November 2020; Received in revised form 26 November 2020; Accepted 1 December 2020

https://doi.org/10.1016/j.giant.2020.100040

membrane permeability, and strong immunogenicity [1–3]. On the other hand, the severe systemic toxicity of chemotherapeutics makes them dose-limiting with narrow therapeutic index [4]. Moreover, both small molecules and proteins often have short circulating half-lives and suboptimal pharmacokinetics (PK). To solve these problems, polymer conjugation (*e.g.*, PEGylation) has been a clinic-validated approach improving pharmacological profiles of both proteins and small molecules [5–9]. Presumably, the attachment of a polymeric chain augments the overall solubility and hydrodynamic volume of drugs, alters the biodistribution, enables sustained release, and leads to slower renal clearance and reduced immunogenicity. Currently, there have been a dozen PEGylated conjugates on market and approximately 30 PEGylated drugs in clinical trial [9].

Combinatory administration of different drugs can sometimes offer a synergistic antitumor effect beyond simple one plus one [10,11]. Clinically, the combination of fluoropyrimidine-cisplatin and bevacizumab significantly increased progression-free survival and overall response rate in the first-line treatment of advanced gastric cancer [12]. Carefully designed co-delivery systems allowing modulable incorporation and fine-tuned release profiles of both the protein and chemodrug payloads have also attracted vast research efforts recently [13–18]. However, the drastic differences in PK, biodistribution, potency, and other related physicochemical properties of small molecules and biologics have posed formidable formulation challenges for maximized codelivery efficacy. Compared with conventional bolus administration or some nanomedicines that loads drugs via physical encapsulation or inclusion [19–21], covalently modified conjugates can largely prevent premature leaking of payloads and thus ensure sustained release of the bioactive components in a spatiotemporally controllable manner. One type of such carriers is the protein-drug-polymer (PDP) conjugate simultaneously armed with both therapeutic modalities within one molecular scaffold. For example, Alexander et al. developed albumin−polymer−drug conjugates to achieve long circulating and high drug loading [22]. However, this seemingly simple and appealing approach has not been widely applied, presumably because the tremendous synthetic challenges of making well-defined PDP conjugates in a controllable fashion.

Herein, we report the highly efficient synthesis of a designer PDP conjugate, which contains a therapeutic human interferon-α2b (IFN), a polydisulfide (PDS) tethering multiple copies of doxorubicin (Dox), and a stealthy polypeptide poly(γ-(2-(2-(2-methoxyethoxy)ethoxy)ethyl $_L$-glutamate) (P(EG_3Glu)) **(Fig. 1)**. The PDP conjugate, termed as IFN-PolyDox-PEP, has an exceedingly high Dox/IFN molar ratio up to 103/1, which is unprecedented using conventional conjugation methods. IFN-PolyDox-PEP is designed to possess long circulation and release its therapeutic cargos through multiple stimuli-responsive mechanisms in tumor microenvironment (TME) and inside tumor cells. Specifically, IFN can be released upon proteolytic cleavage by matrix metalloprotease (MMP) overexpressed TME for enhanced binding to cell surface receptor and thus restored protein activity. Free Dox can be released intracellularly through the degradation of PDS by glutathione (GSH) and the acid-triggered hydrolysis of hydrazide-ketone bond in the endosome/lysosome [23–25]. Notably, such a sophisticatedly designed conjugate can be efficiently prepared within 4 steps thanks to the mild yet efficient chemistry.

Results and discussion

Design, synthesis, and characterization of the conjugate IFN-PolyDox-PEP

IFN is an important cytokine exhibiting anti-proliferative effect to certain types of tumor cells by binding to specific extracellular receptors on the membrane; Dox, a well-known first-line anthracycline drug, induces the apoptosis of a wide spectrum of tumor cells by intercalating with nuclear DNA. We selected IFN and Dox to construct the PDP conjugate because several clinical trials and preclinical studies have demonstrated certain degrees of synergistic efficacy using combinatory regimens of IFN with Dox [26-28]. To make a viable co-delivery construct in which both drugs can act at their optimal doses, we sought to tune the IFN/Dox molar ratio in the conjugate ~1/100 based on reported animal studies in which IFN was used at ~ 50 nmol (1 mg)/kg for IFN[29-31] and ~5 μmol (3 mg)/kg for Dox [13,32,33]. This high Dox/IFN ratio represents a practical synthetic challenge because Dox is relatively hydrophobic and too many copies of Dox in one conjugate may cause undesired precipitation. For this, the hydrophilic and stealthy polypeptide P(EG_3Glu) was firstly introduced for improved solubility and extended circulation half-life. Briefly, Cys-M-IFN, an IFN mutant containing an *N*-terminal cysteine (*N*–Cys) followed by a MMP-responsive peptide linker (sequence: GPLG⁞VRGK), was constructed [30] and reacted with phenyl thioester-tethered P(EG_3Glu)$_{100}$ via native chemical ligation **(Fig. 1A)** [29,31,34–37]. The resulting conjugate IFN-PEP has a reactive thiol group originated from the previous *N*–Cys, which allows the *in situ* growth of PDS through the ring-opening polymerization (ROP) of 1,2-dithiolane [38]. Previously, protein-initiated ROP of 1,2-dithiolane has been elusive. However, by employing the Cryo-ROP method recently developed by our group, this synthetic challenge became easily conquerable. Specifically, the thiol-bearing IFN-PEP was mixed with a hydrazide-functionalized lipoic acid (LA-$NHNH_2$, characterization see Figure S1-S3) under frozen conditions to afford the product IFN-PDS-PEP. Non-reducing SDS-PAGE analysis and size exclusion chromatography (SEC) confirmed the successful generation of IFN-PDS-PEP **(Fig. 2A-B)**. Dynamic light scattering (DLS) result indicated a substantial increase of the hydrodynamic size from 14 nm for IFN-PEP to 28 nm for IFN-PDS-PEP **(Fig. 2C)**. The degree of polymerization (DP) of PDS was estimated to be ~120 based on the assessment of the hydrazide groups in IFN-PDS-PEP using the trinitrobenzene sulfonic acid (TNBS) assay.

Next, Dox was covalently attached to IFN-PDS-PEP via an acid-labile hydrazone bond between the hydrazide of PDS and the ketone of Dox (**Fig. 1A**). The product IFN-PolyDox-PEP was purified by extensive dialysis and was estimated to have a Dox/IFN ratio of ~103 calculating from the absorption intensity of the characteristic wavelengths of Dox and IFN at 495 and 280 nm, respectively. Notably, the purified IFN-PolyDox-PEP showed no leakage of Dox even after one month of storage at 4 °C. This observation further underscored the remarkable stability and high

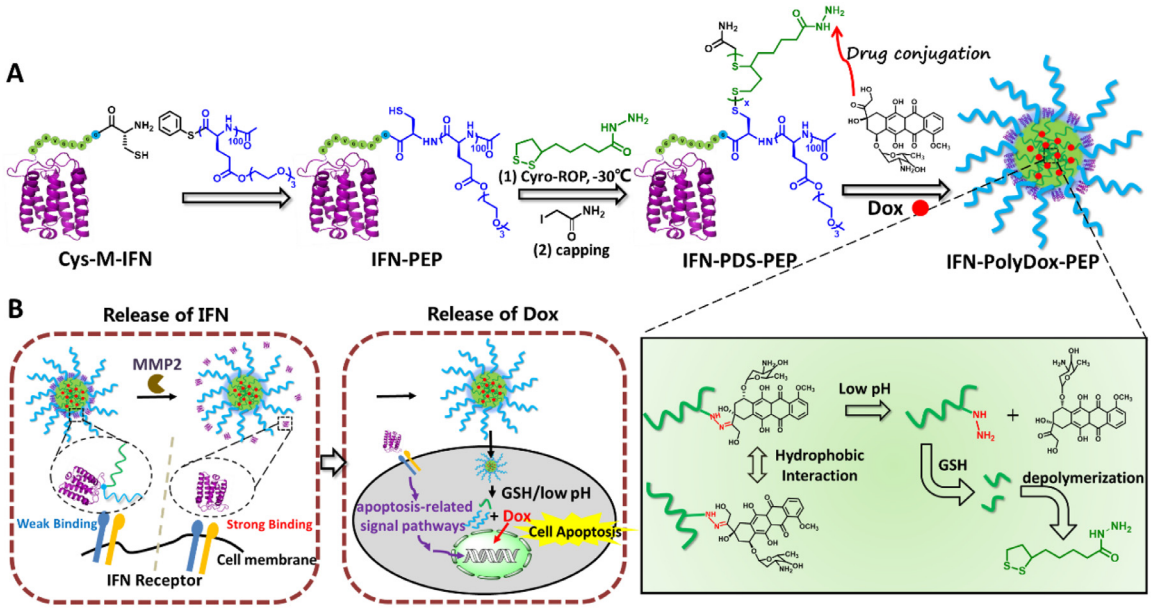

Fig. 1

(A) Synthesis of IFN-PolyDox-PEP. (B) Cartoon illustration of the MMP-activatable, pH- and GSH-responsive release of IFN and Dox for enhanced chemo–protein combination therapy. Cyro-ROP, cryo ring-opening polymerization; Dox, doxorubicin; IFN, interferon-α2b; PDS, polydisulfide; MMP2, matrix metalloproteinase2; GSH, glutathione.

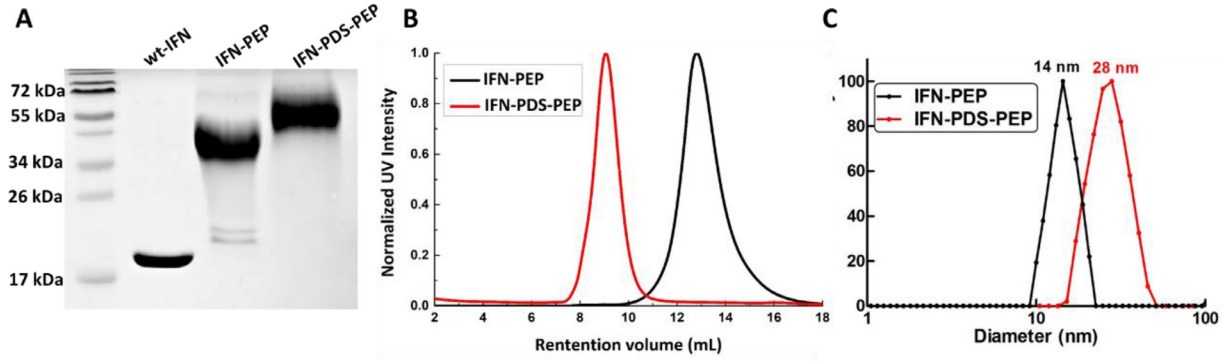

Fig. 2

Characterizations: (A) SDS-PAGE, (B) size exclusion chromatography, and (C) DLS analysis of the precursor IFN-PEP and the PDP conjugate IFN-PDS-PEP. In (A), wt-IFN and IFN-PEP were treated with DTT before electrophoresis, whereas IFN-PDS-PEP was analyzed without DTT.

purity of IFN-PolyDox-PEP. DLS analysis of IFN-PolyDox-PEP gave an average hydrodynamic diameter of 122 nm (**Fig. 3A**), likely due to the self-assemble of the conjugated PolyDox. This result was further confirmed by transmission electron microscopy (TEM), which gave an estimated average size of ~80 nm for IFN-PolyDox-PEP in dry state (**Fig. 3A inset**). Next, we interrogated the stimuli-responsive Dox release of IFN-PolyDox-PEP in phosphate buffer saline (PBS) at 37 °C under different conditions. Since the MMP-specific cleavability of a similar PEPylated interferon, PEP_{20}−M-IFN has been systematically demonstrated in our previous work [30], here, we focused on the responsive release of Dox in this system. As illustrated in **Fig. 3B**, at pH 7.4, only less than 2% Dox was released over 64 h. At pH 6.0 which mimics the slightly acidic TME, the percentage of Dox release increased to 10% owing to the acid-catalyzed hydrolysis of hydrozone bond. Remarkably, in the presence of 10 mM glutathione (GSH), nearly 55% Dox was liberated over a course of 64 h. The results suggested that the Dox release would be further boosted inside the reductive cytosolic milieu for GSH-assisted depolymerization of PDS.

***In vitro* Cytotoxicity.** The *in vitro* cytotoxicity of IFN-PolyDox-PEP was evaluated using the human ovarian cancer cell line SKOV3. Previously, we have observed that SKOV3 was only moderately sensitive to the treatment of IFN both *in vitro* and *in vivo*. Here, we would like to test whether a synergistic effect can be achieved by combinatory therapy of IFN and Dox [14]. As expected, the treatment of Dox + IFN-PEP mixture resulted in significantly lowered viabilities of SKOV3 in relative to Dox or IFN-PEP treatment alone. The conjugate IFN-PolyDox-PEP revealed a slightly lower *in vitro* toxicity as compared to the treatment of Dox + IFN-PEP mixture, which could be attributed to the gradual release of IFN and Dox **(Fig. 4A)**. Next, we examined the intracellular delivery of IFN-PolyDox-PEP by using confocal laser

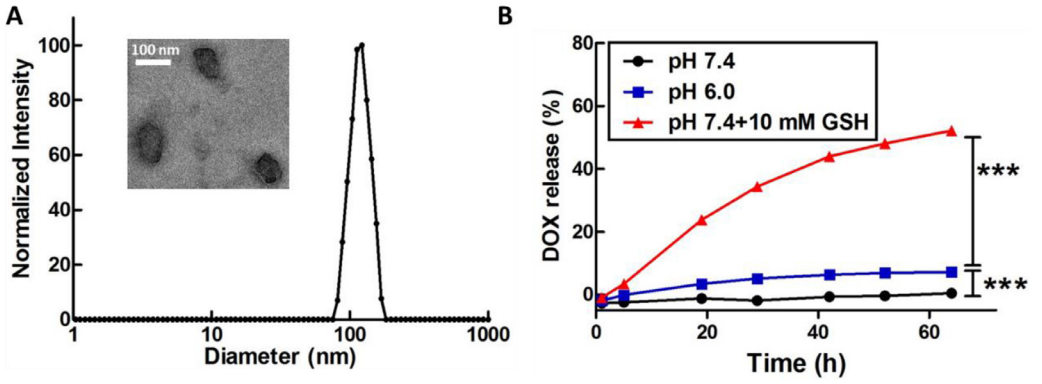

Fig. 3

(A) DLS analysis and TEM images (inset) of IFN-PolyDox-PEP. (B) Dox release profile of IFN-PolyDox-PEP under different conditions (PBS buffer at 37 °C). Each point was based on triplicated experiments and data are presented as mean ± SD ($n = 3$); P value was determined by two-way ANOVA analysis: $^{*}P<0.05$, $^{**}P<0.01$, $^{***}P<0.001$.

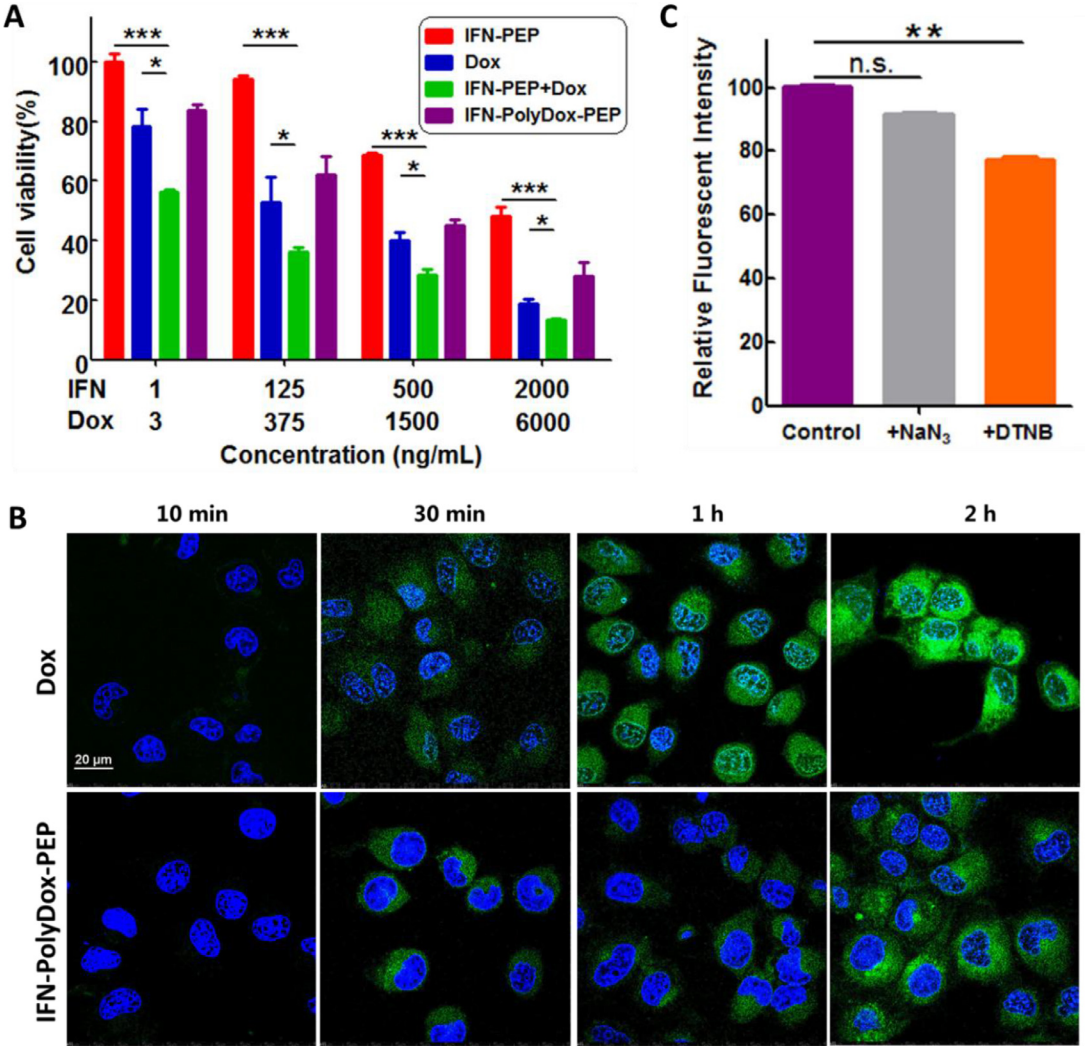

Fig. 4

In vitro Cytotoxicity and cellular uptake: (A) Relative cell viability of SKOV3 cells 48 h after the treatment of IFN-PEP, Dox, Dox + IFN-PEP mixture, or IFN-PolyDox-PEP. (B) CLSM of SKOV3 cells uptaking free Dox or IFN-PolyDox-PEP at different time points. The nucleus is stained with Hochest (blue); Dox is presented in green. (C) Relative uptake of IFN-PolyDox-PEP by SKOV3 cells with different pretreatments. Cells were treated with opti-MEM, sodium azide (10 mM), or DTNB (5 mM) for 30 min before incubation with IFN-PolyDox-PEP (20 μM Dox) for 2 h; Internalization of IFN-PolyDox-PEP were quantified based on the mean fluorescence intensity (MFI) of Dox in flow cytometry histogram. Data are presented as mean ± SD ($n = 3$); P value was determined by t-test: $^{*}P<0.05$, $^{**}P<0.01$. n.s., not significant.

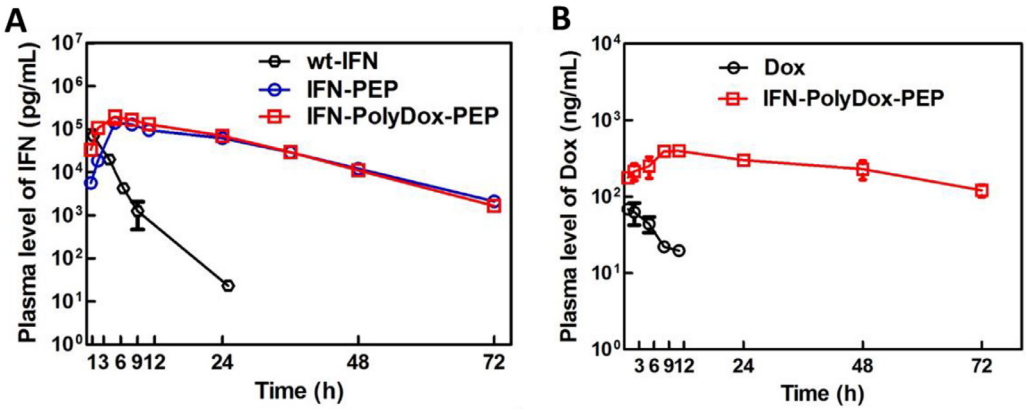

Fig. 5

In vivo pharmacokinetics of Dox + IFN-PEP mixture and IFN-PolyDox-PEP. The plasma level of IFN (A) and Dox (B) at designated time points were measured by anti-IFN ELISA and fluorescence assay, respectively; drugs were intraperitoneally administered to Sprague-Dawley rats and the blood was drawn from the orbit at designated time points. Data are presented as mean ± SD.

scanning microscopy (CLSM) at various time points. As expected, free Dox was internalized into SKOV3 cells more efficiently than IFN-PolyDox-PEP, as shown by the higher intracellular intensity of Dox fluorescence at each incubation time. It is worth mentioning, however, that a substantial amount of Dox signal was distributed throughout the cytosol with no significant endosome/lysosome trapping even at as early as 30 min or 1 h incubation for IFN-PolyDox-PEP **(Fig. 4B)**. It is well-known that nanomedicines are usually uptaken by endocytosis/pinocytosis and can be easily trapped within endosomes/lysosomes. Thus, this difference in subcellular location with vast majority nanomedicines suggested a distinct internalization mechanism and intracellular trafficking of IFN-PolyDox-PEP. Matile and coworkers have convincingly demonstrated that PDS penetrates into cell cytosols through the thiol-initiated disulfide exchange on cell surface, which bypasses conventional endocytosis pathways [25, 39–41]. To investigate the internalization mechanism of IFN-PolyDox-PEP, SKOV3 cells were pretreated with 10 mM sodium azide to inhibit endocytosis or 5,5′-dithiobis-2-nitrobenzoic acid (DTNB) to block cell surface thiols [23,42,43]. Interestingly, the intracellular fluorescence of Dox did not show a dramatic decrease for NaN_3 treatment (n.s.); on the contrary, the thiol-blocking DTNB treatment suppressed ~25% Dox uptake ($P < 0.01$). The results suggested that endocytosis was not the dominate internalization pathway for IFN-PolyDox-PEP and the disulfide exchange-mediated cell-penetrating was at least one accountable internalization mechanism along with others **(Fig. 4C)**.

Pharmacokinetics. To assess the circulation half-life, Sprague-Dawley rats were intraperitoneally administered with either a physically mixed solution of (Dox + IFN-PEP) or the conjugate IFN-PolyDox-PEP. The plasma levels of IFN and Dox were determined by enzyme-linked immunosorbent assay (ELISA) and fluorescence assay, respectively. As shown in **Fig. 5A**, wt-IFN was quickly cleared from blood upon injection and became undetectable within 24 h, whereas both conjugates IFN-PEP and IFN-PolyDox-PEP showed significantly higher plasma IFN contents and were almost indistinguishable with each other throughout all selected time points. The pharmacokinetic profiles of Dox were shown in **Fig. 5B**. Free Dox was cleared rapidly from blood, whereas Dox was maintained at high concentrations even 72 h post injection for IFN-PolyDox-PEP. These results clearly demonstrated the benefit of IFN-PolyDox-PEP in prolonging the circulation time of both therapeutic components for optimal codelivery.

***In vivo* efficacy.** The antitumor efficacy of IFN-PolyDox-PEP was studied in a SKOV3 xenograft model in nude mice. When the average tumor size reached approximately 60 mm^3, mice were randomly grouped ($n = 5–6$) and intravenously administered with phosphate buffer saline (PBS), Dox, IFN-PEP, Dox+IFN-PEP, or IFN-PolyDox-PEP every 4 days at a dosage of 3.0 mg Dox/kg or 1.0 mg IFN/kg per mouse (day 0). As shown in **Fig. 6A**, the tumor grew rapidly in both the Dox and IFN-PEP groups, with no significant difference detected between the two. Notably, the co-injection of Dox and IFN-PEP was found to exhibit significantly higher efficacy of tumor inhibition than individual therapy of IFN-PEP or Dox. IFN-PolyDox-PEP displayed the most remarkable antitumor efficacy and almost completely eradicated the tumor. This result underscored the necessity of both long circulation and chemo-protein combination therapy for suppressing the tumor growth. In the survival study, no mice in the PBS, Dox and IFN-PEP groups remained alive on day 16 due to oversized tumors, whereas those receiving mixture of Dox and IFN-PEP showed slightly extended survival to day 20. To our excitement, none of the mice administered with IFN-PolyDox-PEP died within 27 days **(Fig. 6B)**. The outstanding performance of IFN-PolyDox-PEP in anticancer efficacy was further confirmed by hematoxylin and eosin (H&E) staining of tumor tissue **(Fig. 6C).** H&E staining showed that the tumor treated with PBS consisted of tightly packed tumor cells **(Fig. S4)**, while the tumor treated with free Dox or IFN-PEP exhibited moderate vacuolization. As expected, both IFN-PolyDox-PEP and Dox + IFN-PEP mixture caused higher degrees of tumor cell apoptosis than administration of IFN or Dox individually. No significant body weight loss was observed for all treatments because of the judiciously chosen dosages of IFN and Dox **(Fig. 6D)**. Moreover, IFN-PolyDox-PEP showed no damage to other major tissues (*e.g.* kidney,

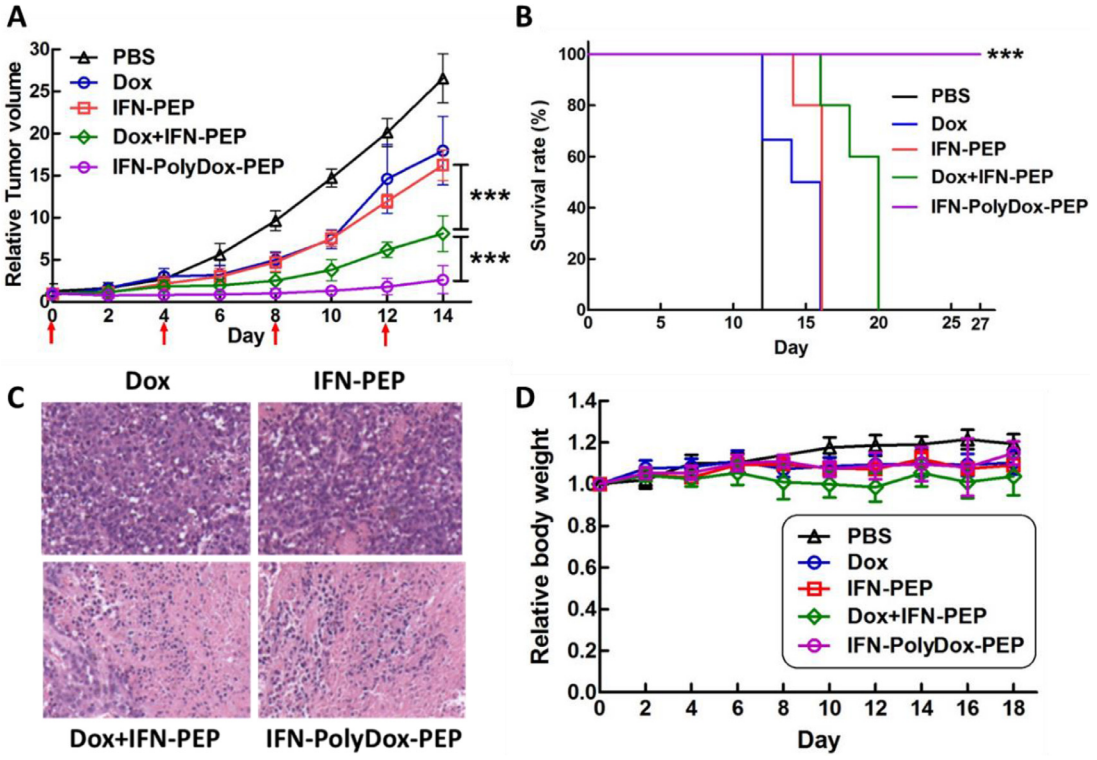

Fig. 6

Antitumor efficacy in SKOV-3 tumor-bearing mice. (A) Tumor growth inhibition curves, (B) survival curve, (C) relative body weight, and (D) H&E-stained tumor sections. BALB/C-nu mice (n = 5–6) bearing s.c. SKOV-3 tumors (~60 mm^3) were i.v. injected with Dox-based therapies at 3.0 mg/kg, or IFN-based therapies at 1.0 mg/kg every 4 days for 4 times; therapies started on day 0 and stopped on day 12. Data are presented as mean ± SD; P value was determined by two-way ANOVA analysis: $^{*}P<0.05$, $^{**}P<0.01$, $^{***}P<0.001$.

spleen, lung and heart) according to the histopathology imaging **(Fig. S5)**.

Conclusions

In summary, we report a well-defined PDP conjugate IFN-PolyDox-PEP to achieve enhanced chemo-protein combination therapy. The construct was facilely prepared via an integrated process harnessing the power of site-specific bioconjugation (grafting-to), in-situ growth of PDS (grafting-from), and hydrazide-ketone chemistry (Dox functionalization). The PDP conjugate bears an exceedingly high Dox loading, self-assembles into nanoparticles ~80–100 nm, circulates in blood for a prolonged time period than individual IFN/Dox, and exhibits multiple stimuli-responsiveness to selectively and sustainably release cargos in TME or inside tumor cells. Consequently, IFN-PolyDox-PEP gives superior *in vivo* antitumor efficacy to simple co-administration of IFN-PEP and Dox. Taken together, this work demonstrates the power of highly efficient chemistry in constructing well-defined PDP conjugates. The method is also easily translatable to other combinations of protein and chemodrugs for treating numerous diseases.

Methods

Synthesis of IFN-PDS-PEP. First, the macroinitiator IFN-PEP was prepared via native chemical ligation of Cys-M-IFN and $P(EG_3Glu)_{100}$-SPh based on a previously reported protocol [30]. LA-$NHNH_2$ (13 mg, 59 μmol) was dissolved in DMSO (100 μL) followed by dilution with PBS (400 μL, pH 7.4) to make the final LA-$NHNH_2$ concentration of ~100 mM. Next, IFN-PEP (1.0 mg/mL, 1.0 mL in PBS) was added to the above LA-$NHNH_2$ solution (100 mM, 500 μL) and the mixture was frozen in a −30 °C freezer for 2 h. The reaction was quenched with cold iodoacetamide (20 μL × 0.5 M) for ~20 min. The reaction mixture was first passed through a PD-10 size exclusion column in PBS (pH 7.4) to remove the unreacted LA-$NHNH_2$. The product IFN-PDS-PEP was further purified via FPLC on a superdex 200 size exclusion column. To analyze the ratio of LA-$NHNH_2$/IFN in the conjugate via the TNBS assay, 20 μL of IFN-PDS-PEP (IFN concentration = 0.75 mg/mL) was incubated with 180 μL of 0.1% (w/v) TNBS in 0.1 M $NaHCO_3$ (pH=8.5) at 37 °C for 120 min. IFN-PEP was used as a blank control to subtract the absorption derived from ε-amine of IFN. Solutions of LA-$NHNH_2$ at different known concentrations in 0.1 M $NaHCO_3$ buffer were used to obtain a calibration curve. The absorbance at 425 nm was recorded using a plate reader.

Synthesis of IFN-PolyDox-PEP. For drug conjugation, Dox (5.0 mg) was dissolved in DMSO (400 μL) followed by the addition of PBS (3.0 mL, pH 7.4) to make a clear aqueous solution. Then IFN-PDS-PEP in PBS (IFN concentration 0.3 mg/mL, 3.5 mL) was added dropwise into the above Dox solution, and the mixture was stirred at room temperature for 24 h in the dark. The final product IFN-PolyDox-PEP was purified by extensive dialysis in PBS to remove DMSO and free Dox (MWCO = 3.5 kDa).

Evaluation of Dox conjugation efficiency. The IFN concentration of IFN-PolyDox-PEP was further confirmed by human IFN ELISA Kit. The concentration of Dox was determined by the absorbance at 495 nm based on a standard curve drawn from a series of free Dox with known concentrations. The ratio of Dox/IFN in the freshly prepared IFN-PolyDox-PEP was calculated based on the c(Dox)/c(IFN).

Dox release studies. IFN-PolyDox-PEP (280 μM Dox, 0.5 mL) in PBS (pH 7.4) were placed in a dialysis tube (MWCO 4 kDa) and dialyzed against PBS (pH 7.4), PBS (pH 6.0), or PBS with GSH (10 mM, pH 7.4) at 37 °C, respectively. The concentration of released Dox were measured at designated time points by taking aliquots of PBS outside the dialysis tube and recording the absorbance at 495 nm based on a standard curve drawn from a series of free Dox with known concentrations. Each experiment was repeated three times.

***In vitro* Cytotoxicity.** SKOV3 cells were cultured in RPMI 1640 supplemented with 10% fetal bovine serum (FBS), 100 U/mL penicillin and 100 U/mL streptomycin. SKOV3 cells were cultured in a 96-well plate at a density of 5000 per well for 24 h before the addition of Dox, IFN-PEP, or IFN-PolyDox-PEP at gradient concentrations with triplicate repeats, respectively. After 48 h incubation, the cell proliferation inhibition was determined by Cell Titer-Blue® Viability Assay. The IC_{50} values were calculated using the GraphPad Prism software.

Cellular uptake of Dox-loaded nanoparticle. SKOV3 cells were cultured in glass bottomed chambers at a density of 50,000 cells per well. After 12 h incubation, the medium was removed and the attached cells were treated with fresh opti-MEM (1.0 mL) containing Dox or IFN-PolyDox-PEP (20 μM based on Dox) at 37 °C. At different time points (10 min, 30 min, 1 h and 2 h), the cells were washed with heparin sodium (0.1 mg/mL, 1.0 mL × 3) and PBS (1.0 mL) and then stained with Hoechst 33,342 at 37 °C. The cells were then washed with PBS three times and then imaged with confocal laser scanning microscope.

Mechanistic studies of cellular internalization

DTNB blocking: SKOV3 cells were seeded in a 6-well dish at a density of 1.0×10^4 cells per well. After 12 h incubation, the medium was removed and the attached cells were treated with fresh opti-MEM (1.0 mL) containing 5 mM DTNB at 37 °C for 30 min. After incubation, the cells were washed with PBS (1.0 mL × 3) and then treated with IFN-PolyDox-PEP (20 μM based on Dox) for 2 h. Then, cells were washed with heparin sodium (0.1 mg/mL, 1.0 mL × 3) and PBS (1.0 mL) and digested with trypsin. Finally, the cells were analyzed by flow cytometry.

NaN_3 Inhibition: For endocytosis inhibition experiment, the cells were incubated with fresh opti-MEM (1.0 mL) containing 10 mM sodium azide (NaN_3) for 30 min at 37 °C. Then, cells were treated with IFN-PolyDox-PEP (20 μM based on Dox). Upon 2 h incubation at 37 °C, cells were washed with heparin sodium (0.1 mg/mL, 1.0 mL × 3) and PBS (1.0 mL) and then digested with trypsin. Finally, the cells were analyzed by flow cytometry.

Pharmacokinetics. The female Sprague-Dawley rats weighing ~250 g were randomly divided into three groups ($n = 3$) and intraperitoneally injected with wt-IFN, IFN-PolyDox-PEP or physically mixed solution of Dox+IFN-PEP at a dose of 50 μg IFN and 150 μg Dox per mouse. At designated time points (45 min, 2, 5, 8, 12, 24, 48 and 72 h), blood was withdrawn from the orbit and kept at 4 °C for 30 min, followed by centrifugation at 4500 g for 15 min. The plasma IFN levels were evaluated by human IFN ELISA Kit; The plasma Dox levels were determined via fluorescence at 590 nm with the fluorescence of plasma from untreated mice measured as the background. A series of free Dox solution at known concentrations ranging from 0.25 to 25 ng/mL was used to establish the standard curve for the quantification of Dox concentration.

***In vivo* anti-tumor efficacy using SKOV-3 model.** Female BALB/c nude mice (4-week old, ~15 g) were subcutaneously implanted with 1.5×10^7 SKOV-3 cells dispersed in 0.1 mL PBS. When the tumor size reached ~60 mm^3, mice were randomly assigned to five groups (n = 5~7, Day 0). The tumor-bearing mice were intravenously (i.v.) administered with phosphate buffer saline (PBS), Dox, IFN-PEP, Dox + IFN-PEP, or IFN-PolyDox-PEP every 4 days at a dose of 15 μg IFN (1.0 mg IFN/kg) and 45 μg Dox (3.0 mg Dox/kg) per mouse for 4 times. Tumor volume was calculated by the following formula: $V = L^*W^2/2$. Relative tumor volume was calculated by the formula: $R = V/V_0$, where V_0 was the average tumor volume on Day 0. The mice were sacrificed when the tumor volume reached 1000 mm^3 or beyond. At the end of the fourth injection, one mice from each group was sacrificed to extract major organs and tumors for histopathology evaluation using H&E staining.

Declaration of Competing Interest

There are no conflicts to declare.

Acknowledgements

This work was financially supported by National Key Research and Development Program of China (No. 2016YFA0201400). We thank the grants from National Natural Science Foundation of China (21722401).

Supplementary materials

Supplementary material associated with this article can be found, in the online version, at doi:10.1016/j.giant.2020.100040.

References

[1] Z. Gu, A. Biswas, M. Zhao, Y. Tang, Tailoring nanocarriers for intracellular protein delivery, Chem. Soc. Rev. 40 (7) (2011) 3638–3655.

[2] X. Liu, C. Wang, Z. Liu, Protein-engineered biomaterials for cancer theranostics, Adv. Healthcare Mater. 7 (20) (2018) 1800913.

[3] Y. Lu, W. Sun, Z. Gu, Stimuli-responsive nanomaterials for therapeutic protein delivery, J. Control. Release 194 (2014) 1–19.

[4] S. Wang, P. Huang, X. Chen, Stimuli-responsive programmed specific targeting in nanomedicine, ACS Nano 10 (3) (2016) 2991–2994.

[5] E.M. Pelegri-O'Day, E.-.W. Lin, H.D. Maynard, Therapeutic protein–polymer conjugates: advancing beyond PEGylation, J. Am. Chem. Soc. 136 (41) (2014) 14323–14332.

[6] R. Duncan, M.J. Vicent, Polymer therapeutics-prospects for 21st century: the end of the beginning, Adv. Drug Deliv. Rev. 65 (1) (2013) 60–70.

[7] J. Kopeček, Polymer–drug conjugates: origins, progress to date and future directions, Adv. Drug Delivery Rev. 65 (1) (2013) 49–59.

[8] C. Li, S. Wallace, Polymer-drug conjugates: recent development in clinical oncology, Adv. Drug Deliv. Rev. 60 (8) (2008) 886–898.

[9] I. Ekladious, Y.L. Colson, M.W. Grinstaff, Polymer–drug conjugate therapeutics: advances, insights and prospects, Nat. Rev. Drug Discov. 18 (4) (2019) 273–294.

[10] T.-.C. Chou, Theoretical basis, experimental design, and computerized simulation of synergism and antagonism in drug combination studies, Pharmacol. Rev. 58 (3) (2006) 621.

[11] C. He, Z. Tang, H. Tian, X. Chen, Co-delivery of chemotherapeutics and proteins for synergistic therapy, Adv. Drug Deliver Rev. 98 (2016) 64–76.

[12] A. Ohtsu, M.A. Shah, E.V. Cutsem, S.Y. Rha, A. Sawaki, S.R. Park, H.Y. Lim, Y. Yamada, J. Wu, B. Langer, M. Starnawski, Y.-.K. Kang, Bevacizumab in combination with chemotherapy as first-line therapy in advanced gastric cancer: a randomized, double-blind, placebo-controlled phase III study, J. Clin. Oncol. 29 (30) (2011) 3968–3976.

[13] T. Jiang, R. Mo, A. Bellotti, J. Zhou, Z. Gu, Gel–liposome-mediated co-delivery of anticancer membrane-associated proteins and small-molecule drugs for enhanced therapeutic efficacy, Adv. Funct. Mater. 24 (16) (2014) 2295–2304.

[14] X. Wu, C. He, Y. Wu, X. Chen, J. Cheng, Nanogel-incorporated physical and chemical hybrid gels for highly effective chemo–protein combination therapy, Adv. Funct. Mater. 25 (43) (2015) 6744–6755.

[15] H. He, Y. Chen, Y. Li, Z. Song, Y. Zhong, R. Zhu, J. Cheng, L. Yin, Effective and selective anti-cancer protein delivery via all-functions-in-one nanocarriers coupled with visible light-responsive, reversible protein engineering, Adv. Funct. Mater. 28 (14) (2018) 1706710.

[16] T. Jiang, W. Sun, Q. Zhu, N.A. Burns, S.A. Khan, R. Mo, Z. Gu, Furin-mediated sequential delivery of anticancer cytokine and small-molecule drug shuttled by graphene, Adv. Mater. 27 (6) (2015) 1021–1028.

[17] C.S. Kim, R. Mout, Y. Zhao, Y.-.C. Yeh, R. Tang, Y. Jeong, B. Duncan, J.A. Hardy, V.M. Rotello, Co-delivery of protein and small molecule therapeutics using nanoparticle-stabilized nanocapsules, Bioconjugate Chem. 26 (5) (2015) 950–954.

[18] W.Q. Lim, S.Z.F. Phua, Y. Zhao, Redox-responsive polymeric nanocomplex for delivery of cytotoxic protein and chemotherapeutics, ACS Appl. Mater. Interfaces 11 (35) (2019) 31638–31648.

[19] L. Sun, X. Ma, C.-.M. Dong, B. Zhu, X. Zhu, NIR-responsive and Lectin-binding doxorubicin-loaded nanomedicine from Janus-type dendritic PAMAM amphiphiles, Biomacromolecules 13 (11) (2012) 3581–3591.

[20] H. Cabral, Y. Matsumoto, K. Mizuno, Q. Chen, M. Murakami, M. Kimura, Y. Terada, M.R. Kano, K. Miyazono, M. Uesaka, N. Nishiyama, K. Kataoka, Accumulation of sub-100nm polymeric micelles in poorly permeable tumours depends on size, Nat. Nanotech. 6 (12) (2011) 815–823.

[21] W. Sun, T. Jiang, Y. Lu, M. Reiff, R. Mo, Z. Gu, Cocoon-like self-degradable DNA nanoclew for anticancer drug delivery, J. Am. Chem. Soc. 136 (42) (2014) 14722–14725.

[22] A.A.A. Smith, K. Zuwala, O. Pilgram, K.S. Johansen, M. Tolstrup, F. Dagnæs-Hansen, A.N. Zelikin, Albumin–polymer–drug conjugates: long circulating, high payload drug delivery vehicles, ACS Macro Lett. 5 (10) (2016) 1089–1094.

[23] J. Fu, C. Yu, L. Li, S.Q. Yao, Intracellular delivery of functional proteins and native drugs by cell-penetrating poly(disulfide)s, J. Am. Chem. Soc. 137 (37) (2015) 12153–12160.

[24] L. Qian, J. Fu, P. Yuan, S. Du, W. Huang, L. Li, S.Q. Yao, Intracellular delivery of native proteins facilitated by cell-penetrating poly(disulfide)s, Angew. Chem., Int. Ed. 57 (6) (2018) 1532–1536.

[25] G. Gasparini, E.-.K. Bang, G. Molinard, D.V. Tulumello, S. Ward, S.O. Kelley, A. Roux, N. Sakai, S. Matile, Cellular uptake of substrate-initiated cell-penetrating poly(disulfide)s, J. Am. Chem. Soc. 136 (16) (2014) 6069–6074.

[26] A.O. Kaseb, J. Shindoh, Y.Z. Patt, R.E. Roses, G. Zimmitti, R.D. Lozano, M.M. Hassan, H.M. Hassabo, S.A. Curley, T.A. Aloia, J.L. Abbruzzese, J.-.N. Vauthey, Modified cisplatin/interferon α-2b/doxorubicin/5-fluorouracil (PIAF) chemotherapy in patients with no hepatitis or cirrhosis is associated with improved response rate, resectability, and survival of initially unresectable hepatocellular carcinoma, Cancer 119 (18) (2013) 3334–3342.

[27] A. Argiris, S.S. Agarwala, M.V. Karamouzis, L.A. Burmeister, S.E. Carty, A phase II trial of doxorubicin and interferon alpha 2b in advanced, non-medullary thyroid cancer, Investig. New Drugs 26 (2) (2008) 183–188.

[28] E.M. Dijkgraaf, S.J.A.M. Santegoets, A.K.L. Reyners, R. Goedemans, M.C.A. Wouters, G.G. Kenter, A.R. van Erkel, M.I.E. van Poelgeest, H.W. Nijman, J.J.M. van der Hoeven, M.J.P. Welters, S.H. van der Burg, J.R. Kroep, A phase I trial combining carboplatin/doxorubicin with tocilizumab, an anti-IL-6R monoclonal antibody, and interferon-α2b in patients with recurrent epithelial ovarian cancer, Ann. Oncol. 26 (10) (2015) 2141–2149.

[29] Y. Hou, Y. Zhou, H. Wang, R. Wang, J. Yuan, Y. Hu, K. Sheng, J. Feng, S. Yang, H. Lu, Macrocyclization of interferon–poly(α-amino acid) conjugates significantly improves the tumor retention, penetration, and antitumor efficacy, J. Am. Chem. Soc. 140 (3) (2018) 1170–1178.

[30] H. Wang, Y. Hou, Y. Hu, J. Dou, Y. Shen, Y. Wang, H. Lu, Enzyme-activatable interferon–poly(α-amino acid) conjugates for tumor microenvironment potentiation, Biomacromolecules 20 (8) (2019) 3000–3008.

[31] Y. Hou, Y. Zhou, H. Wang, J. Sun, R. Wang, K. Sheng, J. Yuan, Y. Hu, Y. Chao, Z. Liu, H. Lu, Therapeutic Protein PEPylation, The helix of nonfouling synthetic polypeptides minimizes antidrug antibody generation, ACS Cent. Sci. 5 (2) (2019) 229–236.

[32] Y. Li, L. Yang, Y. Zeng, Y. Wu, Y. Wei, L. Tao, Self-healing hydrogel with a double dynamic network comprising imine and borate ester linkages, Chem. Mater. 31 (15) (2019) 5576–5583.

[33] T. Cui, J.-.J. Liang, H. Chen, D.-.D. Geng, L. Jiao, J.-.Y. Yang, H. Qian, C. Zhang, Y. Ding, Performance of doxorubicin-conjugated gold nanoparticles: regulation of drug location, ACS Appl. Mater. Interfaces 9 (10) (2017) 8569–8580.

[34] Y. Hou, H. Lu, Protein PEPylation: a new paradigm of protein–polymer conjugation, Bioconjugate Chem. 30 (6) (2019) 1604–1616.

[35] J. Yuan, Y. Sun, J. Wang, H. Lu, Phenyl trimethylsilyl sulfide-mediated controlled ring-opening polymerization of α-Amino Acid N-Carboxyanhydrides, Biomacromolecules 17 (3) (2016) 891–896.

[36] Y. Hou, J. Yuan, Y. Zhou, J. Yu, H. Lu, A concise approach to site-specific topological protein–poly(amino acid) conjugates enabled by in situ-generated functionalities, J. Am. Chem. Soc. 138 (34) (2016) 10995–11000.

[37] Y. Hu, Y. Hou, H. Wang, H. Lu, Polysarcosine as an alternative to PEG for therapeutic protein conjugation, Bioconjugate Chem. 29 (7) (2018) 2232–2238.

[38] J. Lu, H. Wang, Z. Tian, Y. Hou, H. Lu, Cryopolymerization of 1,2-dithiolanes for the facile and reversible grafting-from synthesis of protein–polydisulfide conjugates, J. Am. Chem. Soc. 142 (3) (2020) 1217–1221.

[39] G. Gasparini, S. Matile, Protein delivery with cell-penetrating poly(disulfide)s, Chem. Commun. 51 (96) (2015) 17160–17162.

[40] P. Morelli, S. Matile, Sidechain engineering in cell-penetrating poly(disulfide)s, Helv. Chim. Acta 100 (3) (2017) e1600370.

[41] G.S. Pulcu, N.S. Galenkamp, Y. Qing, G. Gasparini, E. Mikhailova, S. Matile, H. Bayley, Single-molecule kinetics of growth and degradation of cell-penetrating poly(disulfide)s, J. Am. Chem. Soc. 141 (32) (2019) 12444–12447.

[42] J. Lu, Y. Zhao, X. Zhou, J.H. He, Y. Yang, C. Jiang, Z. Qi, W. Zhang, J. Liu, Biofunctional polymer–lipid hybrid high-density lipoprotein-mimicking nanoparticles loading anti-miR155 for combined antiatherogenic effects on macrophages, Biomacromolecules 18 (8) (2017) 2286–2295.

[43] A. Okuda, S. Tahara, H. Hirose, T. Takeuchi, I. Nakase, A. Ono, M. Takehashi, S. Tanaka, S. Futaki, Oligoarginine-Bearing tandem repeat penetration-accelerating sequence delivers protein to cytosol via caveolae-mediated endocytosis, Biomacromolecules 20 (5) (2019) 1849–1859.